Transmission and intensity correlations in wave propagation through random media

Johannes F. de Boer and Meint P. van Albada
Natuurkundig Laboratorium, Universiteit van Amsterdam, Valckenierstraat 65, 1018 XE Amsterdam, The Netherlands

Ad Lagendijk
Natuurkundig Laboratorium, Universiteit van Amsterdam, Valckenierstraat 65, 1018 XE Amsterdam, The Netherlands and FOM—Institute for Atomic and Molecular Physics, Kruislaan 407, 1089 SJ Amsterdam, The Netherlands

(Received 24 May 1991)

We report on an experimental study of wavelength-dependent intensity fluctuations in coherent light that passed through a random dielectric medium. For the intensity that is scattered into a narrow solid angle and for the total transmission, we find exponential- and power-law decay in the intensity-intensity and transmission-transmission correlation, respectively. We derive an expression for the intensity-intensity correlation *in* the medium under the prevailing experimental conditions: Gaussian incident beam, slab geometry, and some absorption. From this expression we calculate the short-range and long-range correlation functions, using a Langevin approach to find the latter. Two earlier calculations of the long-range corrrelation function disagreed by a prefactor. The present theory quantitatively describes the long-range correlation, and therefore removes the uncertainty about this factor. With the Boltzmann diffusion constant for light in the random medium as the only fitting parameter, we obtain quantitative agreement between theory and experiment.

I. INTRODUCTION

In recent years interference effects in the multiple scattering of waves in disordered media have raised a lot of interest. Weak localization of electrons has been known for some time.[1] More recently, weak localization of electromagnetic waves has been observed in the form of enhanced backscattering.[2] Intensity fluctuations, possibly related to the "universal" fluctuations known in electronic conduction, have been observed.[3–7] Theoretical results as obtained through a diagrammatic technique[8] and also a random-matrix approach[9] predict that the universal conductance fluctuations (UCF) observed in electron transport,[10] indeed, have an electromagnetic wave counterpart. We shall briefly summarize these results: The volume occupied by the random sample is considered to be a waveguide, supporting N modes. The sample will mutually couple these modes in a random manner, and intensity transmission coefficients $T_{\alpha\beta}$ give the fraction of the power in the incoming mode α that is coupled into the outgoing mode β. For the correlator $C_{\alpha\beta\alpha'\beta'} \equiv \langle \delta T_{\alpha\beta}\, \delta T_{\alpha'\beta'} \rangle$ (angular brackets stand for averaging over the disorder), Feng *et al.*[8] obtained the expression $C = C_1 + C_2 + C_3$ with

$$C^{(1)}_{\alpha\beta\alpha'\beta'} \equiv D_1 \langle T_{\alpha\beta} \rangle \langle T_{\alpha'\beta'} \rangle \delta_{\Delta\mathbf{q}_\alpha, \Delta\mathbf{q}_\beta} F_1(\Delta\mathbf{q}_\alpha L) ,$$

$$C^{(2)}_{\alpha\beta\alpha'\beta'} \equiv D_2 g^{-1} \langle T_{\alpha\beta} \rangle \langle T_{\alpha'\beta'} \rangle [F_2(\Delta\mathbf{q}_\alpha L) + F_2(\Delta\mathbf{q}_\beta L)] ,$$

$$C^{(3)}_{\alpha\beta\alpha'\beta'} \equiv D_3 g^{-2} \langle T_{\alpha\beta} \rangle \langle T_{\alpha'\beta'} \rangle ,$$

where the D's are constants of order unity and F_1 and F_2 are form functions. The C_1 part is of order 1 if $\alpha = \alpha'$ *and* $\beta = \beta'$, and decays exponentially with increasing $\Delta\mathbf{q} \equiv \mathbf{q}_\alpha - \mathbf{q}_{\alpha'} = \mathbf{q}_\beta - \mathbf{q}_{\beta'}$ ("memory effect"), and is zero if $\Delta\mathbf{q}_\alpha \neq \Delta\mathbf{q}_\beta$. The C_2 part is of the order g^{-1} (with g the conductivity Nl/L, where l is the mean free path and L the sample thickness) if *either* $\Delta\mathbf{q}_\alpha$ *or* $\Delta\mathbf{q}_\beta = 0$ and shows power-law decay with increasing $\Delta\mathbf{q}$. Finally, the C_3 part is of the order g^{-2} and does not depend on either $\Delta\mathbf{q}_\alpha$ or $\Delta\mathbf{q}_\beta$. The same types of correlation, short range, long range, and "infinite range," respectively, will show in the corresponding three components of the two-frequency correlator $\langle \delta T_{\alpha\beta}(\omega) \delta T_{\alpha\beta}(\omega') \rangle$ for varying $\Delta\omega \equiv \omega - \omega'$. The results predict that if, in an experiment on a sample with $g \gg 1$, just one incoming mode is excited, the C_1 and C_2 correlation functions will be measured in the signal in just one outgoing mode and the total transmission, respectively. If all incoming modes are excited by mutually uncorrelated signals and the total transmission is measured for different sample realizations (we then have a situation analogous to that in an electronic conduction experiment) the C_3 term (UCF) would be found.

The short-range correlation function C_1 has been studied by varying the angle of incidence[4] and wavelength.[6,7] Its shape does not depend on the beam profile. The long-range correlation function C_2 does depend on the beam profile and has been calculated in the plane-wave limit for both varying angle of incidence[8] and varying wavelength.[11] Long-range correlation has been observed in experiments with varying wavelength in the microwave[5] and optical[7] regions.

In the present paper we describe detailed measure-

ments of both the short-range $[C_1(\Delta\omega)]$ and the long-range $[C_2(\Delta\omega)]$ correlation functions, including the dependence on beam profile of the latter. We also calculate the correlation functions and compare the experimental results with theory.

In Sec. II we derive an expression for the frequency-dependent intensity-intensity correlation in volume speckle within a weakly absorbing random dielectric medium with slab geometry for a Gaussian incident beam. The short-range C_1 correlation function that holds for intensity fluctuations in light that is scattered into a narrow solid angle follows directly from this expression. In Sec. III we calculate the long-range C_2 correlation function that holds for the total transmitted intensity from the short-range correlation function for volume speckle through a Langevin approach.[12] Experimental techniques are described in Sec. IV. The measurement of $C_2(\Delta\omega)$ correlation functions is affected by the finite length of the frequency interval over which scans could be made. We used Fourier techniques to correct for this effect. These techniques are described in Sec. V. In Sec. VI the results are discussed, and conclusions are given in Sec. VII.

II. INTENSITY CORRELATION IN VOLUME SPECKLE

We measure wavelength-dependent intensity-intensity correlation because—at least in the optical region—these are experimentally more accessible than correlations that depend on spatial position or angle of incidence. We shall restrict our calculations to this type of correlations as well.

Because of interference, the intensity inside the (static) random dielectric slab will fluctuate strongly in space ("volume speckle"). In this section we calculate the average correlation in the intensity in a correlation volume (speckle spot) at depth z as a function of the frequency shift in the incident coherent light. The correlation function is defined as

$$C(\omega,\Delta\omega,\mathbf{r})\equiv\frac{\langle I(\omega,\mathbf{r})I(\omega',\mathbf{r})\rangle-\langle I(\omega,\mathbf{r})\rangle\langle I(\omega',\mathbf{r})\rangle}{\langle I(\omega,\mathbf{r})\rangle\langle I(\omega',\mathbf{r})\rangle}\ . \tag{1}$$

From now on we drop the ω dependence in $C(\omega,\Delta\omega,\mathbf{r})$. Writing the diffuse part $\langle I(\omega,\mathbf{r})\rangle$ in its field components, we get

$$\begin{aligned}\langle I(\omega,\mathbf{r})\rangle&\equiv\langle\Psi(\omega,\mathbf{r})\Psi^*(\omega,\mathbf{r})\rangle\\&\equiv\int\cdots\int d\mathbf{r}_1\cdots d\mathbf{r}_4\langle G(\omega,\mathbf{r},\mathbf{r}_1)\rangle\langle G^*(\omega,\mathbf{r},\mathbf{r}_2)\rangle\langle L(\omega,\mathbf{r}_1,\mathbf{r}_2;\mathbf{r}_3,\mathbf{r}_r)\rangle\Psi(\omega,\mathbf{r}_3)\rangle\langle\Psi^*(\omega,\mathbf{r}_4)\rangle\ ,\end{aligned} \tag{2}$$

with $\langle G(\omega,\mathbf{r},\mathbf{r}_1)\rangle$ the average-amplitude Green's function for propagation from $\mathbf{r}_1$ to $\mathbf{r}$ in a disordered medium. The four-point vertex $\langle L\rangle$ denotes the sum of all ladder diagrams. Writing the correlator $\langle I(\omega,\mathbf{r})I(\omega',\mathbf{r})\rangle$ in its field components, we get

$$\begin{aligned}\langle I(\omega,\mathbf{r})I(\omega',\mathbf{r})\rangle&\equiv\langle\Psi(\omega,\mathbf{r})\Psi^*(\omega,\mathbf{r})\Psi(\omega',\mathbf{r})\Psi^*(\omega',\mathbf{r})\rangle\\&\equiv\int\cdots\int d\mathbf{r}_1\cdots d\mathbf{r}_8\langle G(\omega,\mathbf{r},\mathbf{r}_1)\rangle\langle G^*(\omega,\mathbf{r},\mathbf{r}_2)\rangle\langle G(\omega',\mathbf{r},\mathbf{r}_3)\rangle\langle G^*(\omega',\mathbf{r},\mathbf{r}_4)\rangle\\&\quad\times\langle K(\omega,\omega',\mathbf{r}_1,\ldots,\mathbf{r}_4;\mathbf{r}_5,\ldots,\mathbf{r}_8)\rangle\langle\Psi(\omega,\mathbf{r}_5)\rangle\langle\Psi^*(\omega,\mathbf{r}_6)\rangle\langle\Psi(\omega',\mathbf{r}_7)\rangle\langle\Psi^*(\omega',\mathbf{r}_8)\rangle\ .\end{aligned} \tag{3}$$

The eight-point vertex $\langle K\rangle$ contains all possible four amplitude diagrams. Feng *et al.*[8] showed that the intensity correlations of interest can be classified by writing the eight-point vertex $\langle K\rangle$ in an expansion of g^{-1}, where $g=Nl/L$. In the lowest-order expansion, the eight-point vertex $\langle K\rangle$ factorizes as a product of two ladder vertices $\langle L\rangle\times\langle L\rangle$. Higher-order terms of the expansion in g^{-1} contain Hikami boxes,[13] (irreducible) eight-point vertices connecting two ladder vertices, which describe the long-range correlations in volume speckle. In this section we are interested in the short-range correlation only, which follows from the lowest-order expansion of $\langle K\rangle$:

$$\begin{aligned}\langle K(\omega,\omega',\mathbf{r}_1,\ldots,\mathbf{r}_4;\mathbf{r}_5,\ldots,\mathbf{r}_8)\rangle&=\langle L(\omega,\mathbf{r}_1,\mathbf{r}_2;\mathbf{r}_5,\mathbf{r}_6)\rangle\langle L(\omega',\mathbf{r}_3,\mathbf{r}_4;\mathbf{r}_7,\mathbf{r}_8)\rangle\\&\quad+\langle L(\omega,\omega',\mathbf{r}_1,\mathbf{r}_2;\mathbf{r}_5,\mathbf{r}_8)\rangle\langle L(\omega,\omega',\mathbf{r}_3,\mathbf{r}_4;\mathbf{r}_6,\mathbf{r}_7)\rangle\ .\end{aligned} \tag{4}$$

The vertex $\langle L(\omega,\omega')\rangle$ in Eq. (4) denotes the ladder diagrams in which two amplitudes with different frequency travel along the same path. Using Eqs. (2–4), the numerator of the rhs of Eq. (1) may be written as

$$\begin{aligned}&\langle I(\omega,\mathbf{r})\rangle^2C(\Delta\omega,\mathbf{r})\\&\equiv\int\cdots\int d\mathbf{r}_1\cdots d\mathbf{r}_4\langle G(\omega,\mathbf{r},\mathbf{r}_1)\rangle\langle G^*(\omega',\mathbf{r},\mathbf{r}_2)\rangle\langle L(\omega,\omega',\mathbf{r}_1,\mathbf{r}_2;\mathbf{r}_3,\mathbf{r}_4)\rangle\langle\Psi(\omega,\mathbf{r}_3)\rangle\langle\Psi^*(\omega',\mathbf{r}_4)\rangle\\&\quad\times\int\cdots\int d\mathbf{r}_1\cdots d\mathbf{r}_4\langle G(\omega',\mathbf{r},\mathbf{r}_1)\rangle\langle G^*(\omega,\mathbf{r},\mathbf{r}_2)\rangle\langle L(\omega,\omega',\mathbf{r}_1\mathbf{r}_2;\mathbf{r}_3,\mathbf{r}_4)\rangle\langle\Psi(\omega',\mathbf{r}_3)\rangle\langle\Psi^*(\omega,\mathbf{r}_4)\rangle\ .\end{aligned} \tag{5}$$

To calculate the two-frequency vertex $\langle L(\omega,\omega')\rangle$, the time-dependent ladder vertex $\langle L(t,\omega)\rangle$ is needed. The latter has been calculated by using the time-dependent Green's function[14] in the integral equation

$$\langle L\rangle=\langle l\rangle+\langle l\rangle(\langle G\rangle\langle G^*\rangle)\langle L\rangle\ , \tag{6}$$

with $\langle l\rangle$ the lowest-order contribution to the irreducible four-point vertices. If $\langle l\rangle$ is incorrectly assumed to be frequency independent, the value that one obtains for the energy-transport velocity v which occurs in $\langle L\rangle$ is equal to that of the phase velocity. In real samples one may expect the two velocities to be different. The actual velocity of energy transport may be obtained in $\langle L\rangle$ by taking the frequency dependence of $\langle l\rangle$ (and of the self-energy of $\langle G\rangle$) into account.[15] We thus obtain

$$\langle L(t,\omega,\mathbf{r}_1,\mathbf{r}_2;\mathbf{r}_3,\mathbf{r}_4)\rangle=\frac{4\pi v}{l^2(4\pi Dt)^{3/2}}e^{-(\mathbf{r}_1-\mathbf{r}_3)^2/4Dt}\delta(\mathbf{r}_1-\mathbf{r}_2)\delta(\mathbf{r}_3-\mathbf{r}_4)\ , \tag{7}$$

with $D=vl/3$ the Boltzmann diffusion constant. Defining the propagator

$$H_L(t,\mathbf{r},\mathbf{r}_1)\delta(\mathbf{r}_1-\mathbf{r}_2)\equiv\int d\mathbf{r}_3\int d\mathbf{r}_4\langle G(\omega,\mathbf{r},\mathbf{r}_3)\rangle\langle G^*(\omega,\mathbf{r},\mathbf{r}_4)\rangle\langle L(t,\omega,\mathbf{r}_3,\mathbf{r}_4;\mathbf{r}_1,\mathbf{r}_2)\rangle\ , \tag{8}$$

the corresponding two-frequency ladder vertex $\langle L(\omega,\omega')\rangle$ may be obtained as follows: The phase shift that develops between the two waves that travel along the same path results from their difference in wavelength and will be equal to $\exp(i\Delta\omega t)$. Thus

$$\int dt\,H_L(t,\mathbf{r},\mathbf{r}_1)e^{i\Delta\omega t}\delta(\mathbf{r}_1-\mathbf{r}_2)=\int d\mathbf{r}_3\int d\mathbf{r}_4\langle G(\omega,\mathbf{r},\mathbf{r}_3)\rangle\langle G^*(\omega',\mathbf{r},\mathbf{r}_4)\rangle\langle L(\omega,\omega',\mathbf{r}_3,\mathbf{r}_4;\mathbf{r}_1,\mathbf{r}_2)\rangle\ . \tag{9}$$

For the slab geometry, we have

$$H_L(t,z_1,z_2,\mathbf{r}_\perp)=\frac{ve^{-t/\tau_a}}{8\pi lDtL}\sum_{n=-\infty}^{\infty}e^{-\mathbf{r}_\perp^2/4Dt}e^{-\pi^2n^2Dt/L^2}e^{-i\pi nz_1/L}(e^{i\pi nz_2/L}-e^{-i\pi nz_2/L})\ , \tag{10}$$

where L is defined as $L_{\text{slab}}+2z_0$, z_0 is the distance from the slab boundaries at which the diffuse energy density extrapolates to zero, and absorption is introduced through the inelastic mean free time τ_a. Following Akkermans, Wolf, and Maynard,[16] we will assume that all diffuse intensity is generated at a depth l with respect to the physical boundary of the slab. The average diffuse intensity at depth z is then

$$\langle I(\omega,\mathbf{r}_\perp,z)\rangle=\int dt\int dz_1\int d\mathbf{r}_{1\perp}\int d\mathbf{r}_{2\perp}H_L(t,z_1,z,\mathbf{r}_\perp-\mathbf{r}_{1\perp})\delta(\mathbf{r}_{1\perp}-\mathbf{r}_{2\perp})l\delta(z_1-z_i)\langle\Psi_{\text{inc}}(\omega,\mathbf{r}_{1\perp})\rangle\langle\Psi^*_{\text{inc}}(\omega,\mathbf{r}_{2\perp})\rangle\ , \tag{11}$$

with $z_i=l+z_0$ the injection depth. Substituting Eq. (9) in Eq. (5) and decomposing the incoming amplitudes into their plane-wave components, we get

$$\begin{aligned}\langle I(\mathbf{r}_\perp,z)\rangle^2C(\Delta\omega,\mathbf{r}_\perp,z)&=\frac{l^2}{(2\pi)^4}\int d\mathbf{q}_{1\perp}\int d\mathbf{q}_{4\perp}\int d\mathbf{r}_{1\perp}\int dt\langle\Psi_{\text{inc}}\mathbf{q}_{1\perp})\rangle\langle\Psi^*_{\text{inc}}(\mathbf{q}_{4\perp})\rangle e^{-i\mathbf{r}_{1\perp}\Delta\mathbf{q}_{1\perp}}H_L(t,z_i,z,\mathbf{r}_\perp-\mathbf{r}_{1\perp})e^{i\Delta\omega t}\\&\times\int d\mathbf{q}_{2\perp}\int d\mathbf{q}_{3\perp}\int d\mathbf{r}_{2\perp}\int dt\langle\Psi_{\text{inc}}(\mathbf{q}_{3\perp})\rangle\langle\Psi^*_{\text{inc}}(\mathbf{q}_{2\perp})\rangle e^{i\mathbf{r}_{2\perp}\Delta\mathbf{q}_{2\perp}}H_L(t,z_i,z,\mathbf{r}_\perp-\mathbf{r}_{2\perp})e^{-i\Delta\omega t}\ ,\end{aligned} \tag{12}$$

with $\Delta\mathbf{q}_{1\perp}\equiv\mathbf{q}_{4\perp}-\mathbf{q}_{1\perp}$ and $\Delta\mathbf{q}_{2\perp}\equiv\mathbf{q}_{3\perp}-\mathbf{q}_{2\perp}$. We now integrate over t, $\mathbf{r}_{1\perp}$, and $\mathbf{r}_{2\perp}$, respectively, and write the summation in H_L in closed form. Since we are only interested in the average correlation at depth z, Eq. (12) is integrated over $\mathbf{r}_\perp$. Subsequent integration over $\Delta\mathbf{q}_{2\perp}$ gives $\Delta\mathbf{q}_{1\perp}=\Delta\mathbf{q}_{2\perp}$. The short-range correlation in volume speckle as a function of depth in the slab, beam profile, and frequency shift is then given by

$$\begin{aligned}\langle I(z)\rangle^2C(\Delta\omega,z)=\frac{v^2z_i^2}{(2\pi)^2D^2}&\int d\mathbf{q}_{1\perp}\int d\mathbf{q}_{2\perp}\int d\Delta\mathbf{q}_{1\perp}\langle\Psi_{\text{inc}}(\mathbf{q}_{1\perp})\rangle\langle\Psi^*_{\text{inc}}(\mathbf{q}_{1\perp}+\Delta\mathbf{q}_{1\perp})\rangle\langle\Psi_{\text{inc}}(\mathbf{q}_{2\perp}+\Delta\mathbf{q}_{1\perp})\rangle\langle\Psi^*_{\text{inc}}(\mathbf{q}_{2\perp})\rangle\\&\times\frac{\cosh[2(L-z)\gamma_1]-\cos[2(L-z)\gamma_2]}{\cosh(2L\gamma_1)-\cos(2L\gamma_2)}\ ,\end{aligned} \tag{13}$$

with $\gamma_1\equiv(a^2+b^2)^{1/4}\cos(\phi/2)$, $\gamma_2\equiv(a^2+b^2)^{1/4}\sin(\phi/2)$, $a\equiv\Delta\omega/D$, $b\equiv\Delta\mathbf{q}_{1\perp}^2+k_a^2$, $k_a\equiv\sqrt{1/D\tau_a}$, and $\tan\phi\equiv a/b$. Equation (13) holds independently for three orthogonal directions of polarization.

The short-range correlation in the transmitted intensity is determined by interference that takes place in the point of observation, i.e., outside the slab. The two ladder vertices in Eq. (5) will in general have different emission points from where the two intensities propagate to the point of observation. The integrations over $\mathbf{r}_\perp$ must therefore be performed *independently* over the first and second right-hand factor of Eq. (12). This leads to $\Delta\mathbf{q}_{1\perp}=0$ and $\Delta\mathbf{q}_{2\perp}=0$, respectively, so that the short-range correlation function in the transmitted intensity $C_1(\Delta\omega)$, unlike the short-range correlation function in the volume, does not depend on the beam profile. If, in addition, we neglect absorption, we obtain from Eq. (13) the earlier reported[6,11] short-range correlation function

$$C_1(\Delta\omega)=\frac{L^2}{z_f^2}\frac{\cosh[z_f(2a)^{1/2}]-\cos[z_f(2a)^{1/2}]}{\cosh[L(2a)^{1/2}]-\cos[L(2a)^{1/2}]}\ , \tag{14}$$

with $L-z_f$ the emission depth, in analogy with the injection depth z_i.

III. LONG-RANGE CORRELATION

Correlation in the total transmitted intensity may be calculated using a Langevin approach. In this approach, which was first used in the present context by Spivak and Zyuzin,[12] volume speckle acts as a source for a fluctuating flux component $\mathbf{j}_{\rm ext}(\mathbf{r})$, which generates the long-range intensity correlations. Pnini and Shapiro[11] used the method to calculate the intensity-intensity correlation in the total transmission as a function of frequency shift for an incident plane wave. In this section we shall extend the method of Pnini and Shapiro for the case of an incident beam with Gaussian intensity profile. In the Langevin approach the diffusion equation for the fluctuating quantity $\delta I \equiv I - \langle I \rangle$ is

$$D\nabla^2 \delta I(\omega,\mathbf{r}) = \nabla \cdot \mathbf{j}_{\rm ext}(\omega,\mathbf{r}) \ . \tag{15}$$

From Eq. (15) an expression for the long-range correlation function $\langle \delta I(\omega,\mathbf{k}_{1\perp},z_1)\delta I^*(\omega',\mathbf{k}_{2\perp},z_2)\rangle$ is obtained [the Fourier transform in the (x,y) plane is taken], which in our notation reads

$$\langle \delta I(\mathbf{k}_{1\perp},z_1)\delta I^*(\mathbf{k}_{2\perp},z_2)\rangle = D^{-2}\int_0^L dz' \int_0^L dz'' \langle j_{\rm ext}(\omega,\mathbf{k}_{1\perp},z') j^*_{\rm ext}(\omega',\mathbf{k}_{2\perp},z'')\rangle \times [H_D(\mathbf{k}_{1\perp};z_1,z')H_D(\mathbf{k}_{2\perp};z_2,z'')\mathbf{k}_{1\perp}\cdot\mathbf{k}_{2\perp} + H'_D(\mathbf{k}_{1\perp};z_1,z')H'_D(\mathbf{k}_{2\perp};z_2,z'')] \ , \tag{16}$$

where

$$H_D(\mathbf{k}_\perp;z,z') = \frac{\sinh(k_\perp z_<)\sinh[k_\perp(L-z_>)]}{k_\perp \sinh(k_\perp L)} \tag{17}$$

is the diffuse intensity propagator, $z_< \equiv \min[z,z']$, $z_> \equiv \max[z,z']$, and $H'_D(\mathbf{k}_\perp;z,z')$ is the derivative of H_D with respect to its second argument z'. The flux correlator $\langle j_{\rm ext}(\omega,\mathbf{r}) j^*_{\rm ext}(\omega',\mathbf{r}')\rangle$ in Eq. (16) is obtained from the correlation function [Eq. (13)] for volume speckle and the velocity of energy transport v between neighboring correlation volumes. Its decay with increasing frequency shift follows that of the correlation function for volume speckle, and its dependence on $|\mathbf{r}-\mathbf{r}'|$ is replaced by a δ function. The "strength" of this δ function is found by integrating the *spatial* short-range correlation function[17] over space to obtain the correlation volume of one speckle spot (this yields $2\pi l/k_0^2$, with k_0 the wave vector in the medium). It follows that

$$\langle j^i_{\rm ext}(\omega,\mathbf{r}) j^j_{\rm ext}(\omega',\mathbf{r}')\rangle = \delta_{ij}\frac{v^2\pi l}{3k_0^2}\langle I(\mathbf{r})\rangle^2 C(\Delta\omega,\mathbf{r}_\perp,z)\delta(\mathbf{r}_\perp-\mathbf{r}'_\perp)\delta(z-z') \ . \tag{18}$$

The prefactor that we obtain in the right-hand side of Eq. (18) is a factor of 2 lower than the corresponding factor in the paper of Pnini and Shapiro, to make up for the fact that $\mathbf{j}_{\rm ext}(\omega,r)$ consists of two independent polarization components. Another important difference is the appearance of the energy-transport velocity in Eq. (18).

In order to obtain a description that goes beyond the plane-wave solution for the correlation in the total transmission, we now transform Eq. (16) back to real space and integrate over $\mathbf{r}_{1\perp}$ and $\mathbf{r}_{2\perp} \equiv \mathbf{r}_{1\perp} + \Delta\mathbf{r}_\perp$ at $z_1, z_2 = L - z_f$, with $L - z_f$ the emission depth, in analogy with the injection depth z_i:

$$\langle \delta T^2(\Delta\omega)\rangle \equiv \frac{1}{(2\pi)^2}\int\int\int\int \langle \delta I(\omega,\mathbf{k}_{1\perp}L-z_f)\delta I^*(\omega',\mathbf{k}_{2\perp}L-z_f)\rangle e^{i\mathbf{r}_{1\perp}\cdot(\mathbf{k}_{1\perp}-\mathbf{k}_{2\perp})} e^{-i\mathbf{k}_{2\perp}\cdot\Delta\mathbf{r}_\perp} d\mathbf{r}_{1\perp}\, d\Delta\mathbf{r}_\perp\, d\mathbf{k}_{1\perp}\, d\mathbf{k}_{2\perp}$$
$$= (2\pi)^2 \langle \delta I(\omega,\mathbf{k}_{1\perp}=0, L-z_f)\delta I^*(\omega',\mathbf{k}_{2\perp}=0, L-z_f)\rangle \ . \tag{19}$$

Since after the integration over $\mathbf{r}_{1\perp}$ in Eq. (19) it holds that $\mathbf{k}_{1\perp}=\mathbf{k}_{2\perp}$, Eq. (16) depends on the length of the vector $\mathbf{k}_\perp$ only, and the effect of absorption may be introduced by substituting $|\mathbf{k}_\perp| \to (|\mathbf{k}_\perp|^2 + k_a^2)^{1/2}$ with $k_a = \sqrt{1/D\tau_a}$, where τ_a is the inelastic mean free time. Moreover, because $\mathbf{k}_{1\perp}=\mathbf{k}_{2\perp}$, the Fourier transform in the (x,y) plane of the flux correlator [Eq. (18)], which depends on $\mathbf{k}_{1\perp}-\mathbf{k}_{2\perp}$, turns out to be independent of $\mathbf{k}_\perp$ and will read

$$\langle j_{\rm ext}(\omega,\mathbf{k}_{1\perp},z) j^*_{\rm ext}(\omega',\mathbf{k}_{1\perp},z)\rangle = \frac{v^2 l}{12\pi k_0^2}\langle I(z)\rangle^2 C(\Delta\omega,z) \ . \tag{20}$$

Though independent of $\mathbf{k}_{1\perp}$, the flux correlator still depends on the beam profile through the correlation function for volume speckle [see Eq. (13)]. Assuming the incident beam to be Gaussian, we have

$$\langle \Psi_{\rm inc}(\mathbf{r}_\perp)\rangle = \frac{\sqrt{2}}{\rho_0\sqrt{\pi}} e^{-\mathbf{r}_\perp^2/\rho_0^2} \ , \tag{21}$$

and its Fourier transform

$$\langle \Psi_{\rm inc}(\mathbf{q}_{1\perp})\rangle = \frac{\rho_0}{\sqrt{2\pi}} e^{-\mathbf{q}_\perp^2\rho_0^2/4} \ . \tag{22}$$

Integrating over $\mathbf{q}_{1\perp}$ and $\mathbf{q}_{2\perp}$ in Eq. (13), we get

$$\int d\mathbf{q}_{1\perp}\int d\mathbf{q}_{2\perp}\langle\Psi_{\rm inc}(\mathbf{q}_{1\perp})\rangle\langle\Psi^*_{\rm inc}(\mathbf{q}_{1\perp}+\Delta\mathbf{q}_{1\perp})\rangle\langle\Psi_{\rm inc}(\mathbf{q}_{2\perp}+\Delta\mathbf{q}_{1\perp})\rangle\langle\Psi^*_{\rm inc}(\mathbf{q}_{2\perp})\rangle = e^{-\rho_0^2\Delta q_{1\perp}^2/4} . \tag{23}$$

We may now combine all intermediate results to calculate $\langle\delta T^2(\Delta\omega)\rangle$. Using Eqs. (13), (16), (17), (19), (20), and (23) and taking $\mathbf{k}_{1\perp}=\mathbf{k}_{2\perp}=k_a\hat{\mathbf{k}}_{1\perp}$, we get

$$\langle\delta T^2(\Delta\omega)\rangle = \frac{lv^4 z_i^2 z_f^2 k_a^2}{12\pi k_0^2 D^4}\int d\Delta\mathbf{q}_{1\perp}\int_0^L dz'\, e^{-\rho_0^2\Delta q_{1\perp}^2/4}\frac{\cosh[2(L-z')\gamma_1]-\cos[2(L-z')\gamma_2]}{\cosh(2L\gamma_1)-\cos(2L\gamma_2)}\frac{\cosh(2k_a z')}{\sinh^2(k_a L)} . \tag{24}$$

The total transmission $\langle T\rangle$ is obtained by integrating Eq. (11) over $\mathbf{r}_\perp$ at $z=L-z_f$ and yields

$$\langle T\rangle = \frac{vz_i z_f k_a}{D\sinh(k_a L)} . \tag{25}$$

Integrating over z' in Eq. (24), dividing by $\langle T\rangle^2$, and putting for later convenience the energy and phase velocities v and v_ϕ (that are not rigorously known) into one parameter $\alpha=vv_\phi^2/c^3$, we obtain the final result in which the mean free path is eliminated in favor of the diffusion constant:

$$C_2(\Delta\omega)=\frac{\langle\delta T^2(\Delta\omega)\rangle}{\langle T\rangle^2}=\alpha\frac{c\lambda_{\rm vac}^2 L}{32\pi^3\rho_0^2 D}F_2(\Delta\omega) , \tag{26}$$

with

$$F_2(\Delta\omega)\equiv\int d\Delta\mathbf{q}_{1\perp}\frac{\rho_0^2 e^{-\rho_0^2\Delta q_{1\perp}^2/4}}{L[\cosh(2L\gamma_1)-\cos(2L\gamma_2)]}\left[\frac{\gamma_1\sinh(2L\gamma_1)}{\gamma_1^2-k_a^2}-\frac{\gamma_2\sin(2L\gamma_2)}{\gamma_2^2+k_a^2}-\frac{k_a\sinh(2Lk_a)}{\gamma_1^2-k_a^2}-\frac{k_a\sinh(2Lk_a)}{\gamma_2^2+k_a^2}\right] . \tag{27}$$

In the plane-wave limit $\rho_0\gg L$ and in the absence of absorption, Eqs. (27) and (26) reduce to

$$C_2(\Delta\omega)=\frac{3v_\phi^2\lambda_{\rm vac}^2[\sinh(L\sqrt{2a})-\sin(L\sqrt{2a})]}{4\pi^2c^2 l\rho_0^2\sqrt{2a}\,[\cosh(L\sqrt{2a})-\cos(L\sqrt{2a})]} . \tag{28}$$

The integrand of Eq. (27) contains the influences upon the strength of the long-range correlation of the sample thickness L, the spot size (through ρ_0), the inelastic length (through k_a), and both the frequency shift and differential angle of incidence $\Delta\mathbf{q}_\perp$ (through γ_1 and γ_2). The effect of the angular distribution of the incident light upon the measured correlation is incorporated by integrating over $\Delta\mathbf{q}_\perp$. Two limiting cases may be distinguished: First, for large values of $\Delta\omega$, this parameter will dominate γ_1 and γ_2. $F_2(\Delta\omega)$ then decays as $1/(\Delta\omega^{1/2}L)$, while ρ_0 hardly affects its value. At fixed $\Delta\omega^{1/2}L$ and sample composition, the strength of the correlation will be proportional to L/ρ_0^2 [cf. Eq. (26)]. Second, for small values of $\Delta\omega$, $\Delta\mathbf{q}_\perp$ will dominate γ_1 and γ_2. The integrand of $F_2(\Delta\omega)$ will behave as a function of $\Delta\mathbf{q}_\perp L$, and ρ_0 will still be important. At fixed $\Delta\omega^{1/2}L$ (and sample composition) a reduction of ρ_0 (i.e., an increase in the range of $\Delta\mathbf{q}_\perp$) or an increase of L will now weaken the correlation: The top of $C_2(\Delta\omega)$ will flatten.

In the plane-wave limit Eq. (28), our solution differs from the result of Pnini and Shapiro in the prefactor only. Apart from the already mentioned factor of 2 that results from the effect of the transversal nature of the waves, this is due to different definitions of the beam profile.

IV. EXPERIMENT

The experimental setup as used for total transmission experiments is shown schematically in Fig. 1. A Coherent Radiation, Inc. 590 dye laser operating in broadband mode was used as a light source, and its frequency was varied by driving the birefringent filter under computer control. The beam was chopped, spatially filtered, slightly expanded, and then focused onto the sample, which was mounted on an insert, fitting in the porthole of an integrating sphere. Fluctuations in the total transmission were measured by recording the diffuse intensity in the sphere as a function of wavelength. The beam diameter could be varied by changing the position

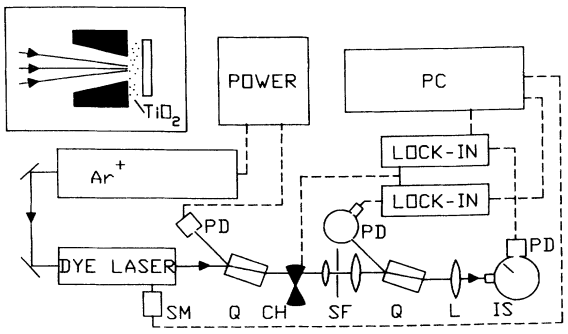

FIG. 1. Experimental setup for the recording of fluctuations in the total transmission. SM, stepper motor; *Q*, quartz beam splitter; CH, chopper; SF, spatial filter; *L* focusing lens; IS, integrating sphere. Inset: Insert as fitted in port of integrating sphere, carrying a sample on transparent supporting material.

of the focusing lens L with respect to the sample and was determined by measuring the distance across the beam between the $1/e$ points with a 10-μm pinhole. The sample-detector assembly was mounted on a translation stage driven by stepper motors under computer control. In each scan, 1024 data points were taken over a wavelength interval between 622 and 583 nm. Between scans, the lateral position of the sample was changed by at least 4 times the beam diameter. A set of scans consisted of 16 consecutive scans probing different parts of a same sample. In the case of C_1-type scans, the integrating detector was replaced by a photomultiplier fitted with a polarizer and a pinhole, positioned at some distance from the sample.

Extreme care was taken to eliminate any fluctuations that are not due to interference effects within the sample: The output of the dye laser was stablized through a feedback circuit coupled to the pump laser (this also minimizes the influence of nonlinearities of the signal and reference detectors and permits the dynamic range of the lock-in amplifier and analog-to-digital converters to be fully exploited over the entire wavelength range). A ratio technique was used to filter out the remaining source fluctuations. The reference photo diode was installed within another integrating sphere because with a parallel incident beam its protective coating was found to produce interference fringes. The recorded (total) transmitted intensity showed a wavelength-dependent drift, resulting from different transmission characteristics of optical components in the signal and reference beams, the wavelength dependence of the average transmission through the sample (l is wavelength dependent), and from different response curves of the detectors. This drift was corrected for by recording a "drift curve" before a set of scans was started, using an unfocused beam in order to average many sample realizations and dividing the recorded curves by this drift curve. We found that, even so, some wavelength-dependent drift remained. Experiments at different power levels showed this remaining drift to be of thermal origin: The focused beam raises the temperature of the probed part of the sample more than does an unfocused beam, and the resulting expansion slightly changes the wavelength dependence of l. Before processing the data, we therefore calculated the average remaining linear drift in the scans belonging to a set and corrected each individual scan for this drift. Part of a genuine linear drift component of the fluctuating intensity is lost in this way.

A typical individual scan is shown in Fig. 2. It is seen that the fluctuating part of the signal appears on top of a large background. Depending on the sample thickness and spot size, relative fluctuations were found ranging form 0.6% to 2.8%. At constant wavelength of the incoming light the relative fluctation was less than 0.05%.

Samples were prepared by suspending rutile TiO_2 pigment in a solution of 3 vol % of PMMA relative to TiO_2 in chloroform. The suspension was then spread on a transparent substrate, and after evaporation of the chloroform, its thickness was determined microscopically. The volume fraction of TiO^2 in the resulting samples was calculated from density determinations to be 36%,

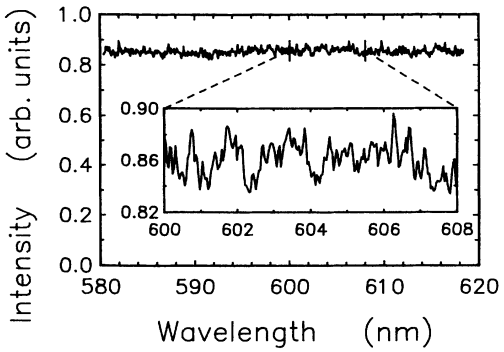

FIG. 2. Total transmission as a function of wavelength for a sample of 30 μm thickness at $\rho_0=26$ μm. The relative fluctuation in the transmission is about 1%.

and the absorption length l_a was determined to be $\simeq 70$ μm.

V. DATA ANALYSIS

In this section we shall discuss some experimental constraints on the measurement of the correlation functions and describe methods that we used to circumvent their effect in the interpretation of the results.

The correlation functions sought are defined as

$$C(\Delta\omega)\equiv\frac{\langle \delta I(\omega)\delta I(\omega')\rangle}{\langle I(\omega)\rangle^2} . \tag{29}$$

Under the experimental conditions (rigid samples), the average over the *disorder* $\langle I(\omega)\rangle$ cannot be obtained, and the best approximation at hand for its value is the average over the *frequency range* $\overline{I(\omega)}$. Since, e.g., the sample thickness may slightly vary with position, $I(\omega)$ values can only be calculated per individual scan. The consequence of using the average over the frequency range instead of that over the disorder is that in a Fourier decomposition of $\delta I(\omega)$ the zeroth component will be missing. Similarly, the linear drift correction discussed in the former section will reduce the first Fourier component and cause some redistribution among a few more low-order components. The combined effect will be mainly a negative offset of the experimental $C(\Delta\omega)$ with respect to the "true" function. In the measurement of $C_1(\Delta\omega)$, this effect is not important, but for $C_2(\Delta\omega)$ it is. In the next section we will therefore compare theoretical $C_2(\Delta\omega)$ curves to both "raw" measured ones and measured ones that were recalculated on the basis of a comparison with theory of all but their lowest Fourier components.

The recalculated correlation functions were obtained as follows: The discrete Fourier transform of $\delta I(\omega_m)$ is defined as

$$\delta I(k_n)\equiv\frac{1}{\sqrt{\Omega}}\sum_{m=0}^{\Omega-1}[I(\omega_m)-\overline{I(\omega)}]e^{ik_n\Delta\omega_m} , \tag{30}$$

with $k_n\equiv 2\pi n/(\omega_{\Omega-1}-\omega_0)$, $n=0,\ldots,\Omega-1$; $\Delta\omega_m$ is m times the frequency step. If we assume $I(\omega_m)$ to be periodic (with periodicity Ω), this definition leads to the following expression for the measured Fourier com-

ponents of $C(\Delta\omega)$:

$$C(k_n)=\frac{1}{\sqrt{\Omega}}[\delta I(k_n)\delta I^*(k_n)/\overline{I(\omega)}^2] . \quad (31)$$

The Fourier transform of $C(\Delta\omega)$ is then defined as

$$C(k_n)\equiv\frac{1}{\sqrt{\Omega}}\left[\sum_{m=0}^{\Omega/2-1} C(\Delta\omega_m)e^{ik_n\Delta\omega_m} + \sum_{m=\Omega/2}^{\Omega-1} C(\Delta\omega_{\Omega-m})e^{ik_n\Delta\omega_m}\right] . \quad (32)$$

It can be seen from Eqs. (27) and (28) that $C_2(\Delta\omega)$ depends on ρ_0 and L, neither of which could be measured with high accuracy. The values used in the calculation of the theoretical $C(k_n)$ may therefore differ somewhat from the actual values. Relatively small errors in ρ_0 and L have a pronounced effect on the vertical scale of the correlation function, but hardly affect its general shape. We therefore corrected for the effects of the finite scan length and drift correction in the following way: For every individual combination of sample thickness and spot size, the calculated curve was fitted to the 4^{th}–300^{th} experimental Fourier component using the D value found in C_1 measurements and a fit-parameter α_{fit} instead of the proportionality constant $\alpha(\equiv v v_\phi^2/c^3)$. We "improved" the set of experimental Fourier components by replacing the first one by its calculated counterpart and adding the calculated zeroth component. The improved set was then transformed back.

VI. RESULTS

In Fig. 3 we present the results of the short-range $C_1(\Delta\omega)$ measurements for samples of 13, 22, 30, and 45 μm in thickness. The scans were made over frequency intervals of 19 113 GHz for the 13- and 22-μm samples and 6371 GHz for the 30- and 45-μm samples, respectively. Using the Boltzmann diffusion coefficient D as a fit parameter, the theoretical curve [Eq. (14)] convolved with the (Gaussian) laser line width of 10 GHz, was fitted to the data points. The smooth curves correspond to a value of $D=12$ m^2 s^{-1}. The horizontal scale was chosen so as to scale out the L dependence of the theoretical curves. Deviations from the resulting "universal" curve are due to the convolution with the laser linewidth. We conclude that Eq. (14) provides a good description of the experimental results.

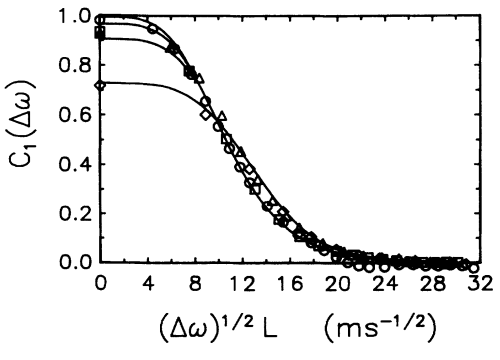

FIG. 3. Comparison of measured $C_1(\Delta\omega)$ correlation functions with theory. Experimental data for ○, $L=13$ μm; □, $L=22$ μm; △, $L=30$ μm; ◇, $L=45$ μm. Smooth lines, theoretical curves as calculated for $D=12$ m^2 s^{-1}, convolved with a laser linewidth of 10 GHz.

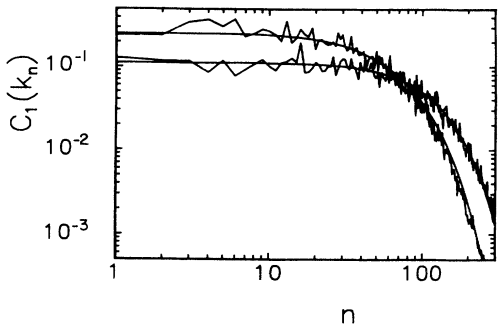

FIG. 4. Comparison of measured $C_1(\Delta\omega)$ correlation functions with theory in the Fourier domain. Upper curve, $L=30$ μm; lower curve, $L=45$ μm. Smooth lines, theoretical curves convolved with a laser linewidth of 10 GHz.

In Fig. 4 we compare theory and experiment for the C_1 correlation function in the Fourier domain. The data correspond to 30- and 45-μm samples, respectively. The measured curves represent $C(k_n)$ averaged over 32 scans, plotted as a function of the Fourier component number. The smooth curves are the calculated $C(k_n)$, obtained by numerically Fourier transforming Eq. (14) after convolving with laser linewidth of 10 GHz. Up to a cutoff that results from the finite slab thickness, the Fourier components of the C_1 correlation function are of equal strength, and this explains why the absence of the zeroth component (cf. Sec. V) is of little importance here.

Figure 5 shows experimental $C_2(\Delta\omega)$ curves as measured for 13-, 30-, 45-, and 78-μm samples using a beam diameter defined by $\rho_0=26$ μm. All scans were made over a frequency range of 31 856 GHz. The choice of the horizontal and vertical scales is such that the theoretical

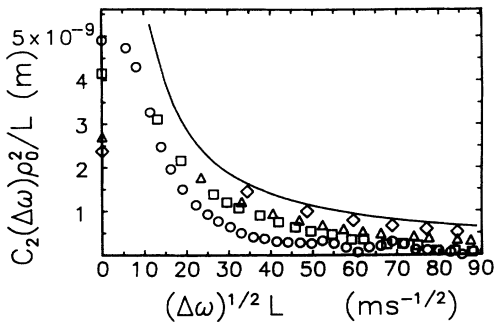

FIG. 5. Raw experimental $C_2(\Delta\omega)$ data as a function of sample thickness at constant beam diameter given by $\rho_0=26$ μm. ○, $L=13$ μm; □, $L=30$ μm; △, $L=53$ μm; ◇, $L=78$ μm. Solid line; "plane-wave limit" ($\rho_0 \gg L$).

curves (only the plane-wave limit is shown) should exhibit a uniform tail. The presented results are averages over 32 scans. All experimental curves indeed show a slowly decaying tail, which, as expected from the absence of the zeroth Fourier component, lies below the theoretical curve. The discrepancy is smaller for the thicker samples because there the relative scan length (the absolute scan length times the square of the thickness) is larger, and consequently the value of $\delta I(\omega)$ is expected to be closer to $\langle \delta I(\omega) \rangle$. The predicted decrease in correlation for small $\Delta\omega$ with increasing slab-thickness, which is due to the finite beam diameter, is indeed found.

Figure 6 shows how theory and experiment compare for the C_2 function in the Fourier domain. The curves correspond to 13- and 53 μm samples, respectively. The measured curves represent the real Fourier components $C_2(k_n)$ averaged over 32 scans and plotted as a function of the Fourier component number. The smooth curves are least-squares fits of the calculated $C_2(k_n)$, with α in Eq. (26) replaced by a fit parameter α_{fit}, to these data points over the 4th up to the 300th Fourier component. The calculated $C_2(\alpha_{\text{fit}}, k_n)$ were obtained by numerically integrating Eq. (27) over $\Delta \mathbf{q}_{1\perp}$ for each frequency shift $\Delta\omega_m$ and numerically Fourier transforming the $C_2(\Delta\omega_m)$ according to Eq. (32).

The presence of a long-range tail in the measured $C_2(\Delta\omega)$ correlation function and its absence in the $C_1(\Delta\omega)$ function are very clearly seen by comparing Figs. 4 and 6. In the C_2 function the magnitude of the Fourier components increases with decreasing component number, whereas in the C_1 function their magnitude is constant.

In Figs. 7 and 8, experimental C_2 correlation functions as obtained by back transformation after correction (cf. Sec. V) of $C(k_n)$ are presented. Figure 7 shows the shape of $C_2(\Delta\omega)$ as a function of the slab thickness at constant beam diameter, and Fig. 8 shows the effect of the beam diameter at constant slab thickness. As mentioned in Sec. V, the fits were made using a fit parameter α_{fit} instead of the proportionality constant α in calculating the theoretical curves. The α_{fit} values found for the various curves are listed in Table I. For clarity, the curves in the figures were all calculated using the average value $\bar{\alpha}=0.10$ (with the chosen x and y scales, this makes the tails coincide). The y values of the data points corresponding to each curve were multiplied by the respective values of $\bar{\alpha}/\alpha_{\text{fit}}$. From Figs. 7 and 8, it is seen that Eqs. (26) and (27) correctly describe the shape of the $C_2(\Delta\omega)$ correlation function, including the influence of L and ρ_0.

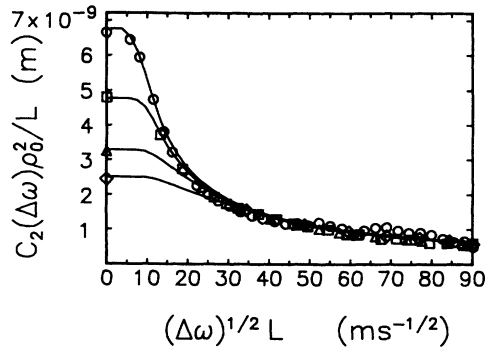

FIG. 7. Recalculated (see text) $C_2(\Delta\omega)$ correlation as a function of sample thickness at constant beam diameter, given by $\rho_0=26$ μm. ○, $L=13$ μm; □, $L=30$ μm; △, $L=53$ μm; ◇, $L=78$ μm. Solid lines, calculated from Eqs. (26) and (27), using $\alpha=0.10$.

We now turn to the vertical scale of the correlation functions. The slight variation in the values of α_{fit} listed in Table I is easily explained in terms of inaccuracies in the values of ρ_0 and L, and in view of the wide range over which these parameters were varied, we conclude that α is indeed a constant. In earlier work different values were found for the constant prefactor in the C_2 function.[11,12] The present results permit the evaluation of this prefactor: Our theory predicts Eq. (26) to hold, and the data show that this expression is directly proportional to the experimental $C_2(\Delta\omega)$ function. If an additional prefactor were involved, it should show up as a proportionality constant between the value of α as defined in Eq. (26) and that of $\bar{\alpha}$ as found from the fit of theory to the data. We therefore calculate α: The velocity of energy transport

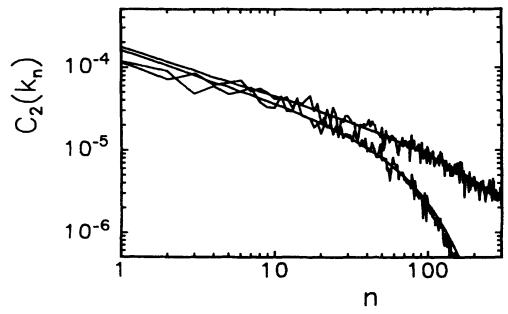

FIG. 6. Comparison of $C_2(\Delta\omega)$ data with theory in the Fourier domain. Upper curve; $L=53$ μm; lower curve, $L=13$ μm; both curves $\rho_0=26$ μm. Smooth lines; least-squares fits of theory to the data over the 4^{th}–300^{th} Fourier component with α as the fit parameter.

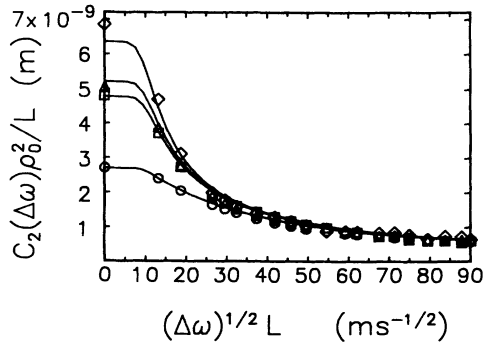

FIG. 8. Recalculated (see text) $C_2(\Delta\omega)$ correlation as a function of beam diameter at constant sample thickness L of 30 μm. ○, $\rho_0=10$ μm; □, $\rho_0=26$ μm; △, $\rho_0=32$ μm; ◇, $\rho_0=74$ μm. Solid lines, calculated from Eqs. (26) and (27), using $\bar{\alpha}=0.10$.

TABLE I. Values of the fit parameter α_{fit} in Eq. (26), given for the specified sample thickness, spot diameter, and number of scans over which it was averaged. Average value $\bar{\alpha}$ of α_{fit} is 0.10.

Sample thickness L (μm)	Beam profile ρ_0 (μm)	Number of scans	α_{fit}
13	26	32	0.087
30	26	32	0.098
53	26	32	0.091
78	26	32	0.106
30	10	32	0.113
30	26	32	0.098
30	32	16	0.117
30	74	16	0.102

between neighboring correlation volumes in our medium by light waves of $\lambda \simeq 600$ nm is low, as a result of resonances in the scattering particles. From independent measurements of l and the mean free time τ_{mf}, we found a value of $v \simeq 5 \pm 1 \times 10^7$ m s^{-1}.[15] A reliable experimental value for the phase velocity in the medium v_ϕ is not available. From Brewster-angle measurements we found $v_\phi = 2.3 \pm 0.2 \times 10^8$ m s^{-1}. This technique, however, probes sample properties very near the surface, which may be different from the bulk properties. Values, estimated on the basis of Mie theory[18] and the Bruggeman effective-medium approximation[19] (the TiO_2 particle diameters are between 130 and 280 nm) fall in the range $2.3 \pm 0.3 \times 10^8$ m s^{-1}. Substitution of these values into the definition of α yields $\alpha \simeq 0.1$, in complete agreement with the value found for $\bar{\alpha}$. We conclude that the description by Eq. (26) is quantitative.

VII. CONCLUSIONS

We have performed a detailed experimental study of correlations in wavelength-dependent intensity fluctuations in light after transmission through random dielectric slabs. In addition, we presented a theoretical model from which both short- and long-range correlations in the transmitted intensity may be calculated. The model incorporates the intensity profile of the incident beam, and its predictions for both the short- and long-range correlation functions are in quantitative agreement with the experimental results.

ACKNOWLEDGMENTS

The authors would like to thank B. van Tiggelen, P. de Vries, M. B. van der Mark, Th. Nieuwenhuizen, and P. Molenaar for helpful discussions. This work was supported in part by the Stichting voor Fundamenteel Onderzoek der Materie (FOM), which is a part of the Nederlandse Organisatie voor Wetenschappelijk Onderzoek (NWO).

[1] G. Bergman, Phys. Rep **107**, 1 (1984); in *Anderson Localization*, edited by T. Ando and H. Fukuyama (Springer-Verlag, Berlin, 1988).

[2] M. P. van Albada and A. Lagendijk, Phys. Rev. Lett. **55**, 2692 (1985); P. E. Wolf and G. Maret, *ibid.* **55**, 2696 (1985). For recent reviews, see S. John, Comments Condens. Matter Phys. **14**, 193 (1988); *Classial Wave Localization*, edited by P. Sheng (World Scientific, Singapore, 1990); *Analogies in Optics and Micro Electronics*, edited by W. van Haeringen and D. Lenstra (Kluwer, Dordrecht, 1990).

[3] A. Z. Genack, Phys. Rev. Lett. **58**, 2043 (1987).

[4] I. Freund, M. Rosenbluh, and S. Feng, Phys. Rev. Lett. **61**, 2328 (1988).

[5] N. Garcia and A. Z. Genack, Phys. Rev. Lett. **63**, 1678 (1989).

[6] A. Z. Genack and J. M. Drake, Europhys. Lett. **11**, 331 (1990).

[7] M. P. van Albada, J. F. de Boer, and A. Lagendijk, Phys. Rev. Lett. **64**, 2787 (1990).

[8] S. Feng, C. Kane, P. A. Lee, and A. D. Stone, Phys. Rev. Lett. **61**, 834 (1988).

[9] P. A. Mello, E. Akkermans, and B. Shapiro, Phys. Rev. Lett. **61**, 459 (1988).

[10] C. P. Umbach, S. Washburn, R. B. Laibowitz, and R. A. Webb, Phys. Rev. B **30**, 4048 (1984).

[11] R. Pnini and B. Shapiro, Phys. Rev. B **39**, 6986 (1989).

[12] B. Z. Spivak and A. Yu. Zyuzin, Solid State Commun. **65**, 311 (1988).

[13] S. Hikami, Phys. Rev. B **24**, 2671 (1981).

[14] D. Vollhardt and P. Wölfle, Phys. Rev. B **22**, 4666 (1980); T. R. Kirkpatrick, *ibid.* **31**, 5746 (1985).

[15] M. P. van Albada, B. A. van Tiggelen, Ad Lagendijk, and A. Tip, Phys. Rev. Lett. **66**, 3132 (1991).

[16] E. Akkermans, P. E. Wolf, and R. Maynard, Phys. Rev. Lett. **56**, 1471 (1986).

[17] B. Shapiro, Phys. Rev. Lett. **57**, 2168 (1986).

[18] See, e.g., H. C. van der Hulst, *Light Scattering by Small Particles* (Dover, New York, 1981), p. 128, or Fig. 4 in Ref. 15.

[19] W. G. Egan and D. E. Aspnes, Phys. Ref. B **10**, 5313 (1982).